Experimental demonstration of kinetic proofreading inherited in ligation-based information replication

Hiroyuki Aoyanagi, Yasuhiro Magi, and Shoichi Toyabe*
Department of Applied Physics, Graduate School of Engineering, Tohoku University, Sendai 980-8579, Japan

(Received 13 May 2025; accepted 23 October 2025; published 8 December 2025)

We experimentally demonstrate that information replication by templated ligation of DNA strands inherits a kinetic proofreading mechanism and achieves significant error suppression through cascade replication. A simple simulation model derived from the experimental results shows that templated ligation has a significant advantage over replication by polymerization for error suppression of long strands. Specifically, longer chains show lower error rates, significantly distinct from the chain-growth polymerization where errors typically accumulate with chain length. This mechanism provides a plausible route for high-fidelity replication in prebiotic chemistry and illustrates how physical principles such as nonequilibrium kinetics and network architecture can drive reliable molecular information replication. The approach also offers strategies for error suppression in biotechnology.

DOI: 10.1103/pdhn-ncpl

I. INTRODUCTION

Accurate replication of information is essential not only to sustain life but also to advance biotechnology. In prebiotic environments, it is not obvious how the fidelity required to maintain genetic information is achieved by primitive error-prone machineries [1–4]. In biotechnology, there is a constant demand to reduce errors, including false positives in virus detection by polymerase chain reaction (PCR) [5] and ligation-based genotyping [6].

In general, replication of a nucleic acid sequence is achieved by aligning short complementary strands to a template and joining them. There are two primary modes of replication, distinguished by how the final product is assembled. The first is chain-growth polymerization, in which monomers are sequentially added until the final product is formed. This mode is ubiquitous in both cells and biotechnologies and has been extensively studied in terms of error suppression [7–12]. However, as the sequence length increases, maintaining high fidelity becomes exponentially more challenging, which limits the maximum sequence length that can be reliably replicated, as explained by the theory of error catastrophe [1].

An alternative replication mode is templated ligation [13–18], where two adjacent short oligomers are joined together on a template (Fig. 1). Templated ligation has recently attracted growing interest as a key reaction mechanism in prebiotic chemistry, owing to its simplicity and its potential to overcome the error catastrophe via emergent higher-order replication [10,14–19]. Templated ligation also has a long history in biotechnology from its use in the ligase chain reaction for single-site error detection [13,20] to more recent applications for synthesizing long DNA or RNA strands [21]. Prominently, information replication by templated ligation can proceed in a cascade manner under nonequilibrium settings of temperature cycling [15,16]. Each ligation step replicates only a partial sequence, but the resulting products can act as substrates in subsequent steps, progressively forming longer sequences. Over multiple steps, the template sequence is fully replicated in the sequence of the product. Recent studies have implicated that this cascade-manner replication enables higher-order replication of information by spontaneously forming cooperative autocatalytic networks [15,19]. This mechanism implies a frequency-dependent selection, which potentially circumvents the error catastrophe observed in chain-growth polymerization. However, errors in cascade replication remain largely unexplored.

In this article, we demonstrate by experiments and simulations that the cascade replication by templated ligation (Fig. 1) inherits a kinetic proofreading mechanism for error suppression. Remarkably, the replication fidelity could increase with sequence length under certain conditions, suggesting the possibility of overcoming the error catastrophe in prebiotic environments and also achieving long-sequence replication with high fidelity in biotechnologies. The kinetic proofreading is a prominent mechanism to achieve fidelity [22–24], where cascade reactions make multiple evaluations of errors and thereby increase the fidelity multiplicatively through cascades. This mechanism is thought to require a complex molecular mechanism, and its implementation in biotechnology is not straightforward [25]. However, our experiments illustrate how physical principles such as nonequilibrium kinetics and network architecture can drive reliable molecular information replication.

II. RESULTS—EXPERIMENTS

We prepared a simple model experimental system to measure the replication dynamics and errors in cascaded ligation

*Contact author: toyabe@tohoku.ac.jp

Published by the American Physical Society under the terms of the Creative Commons Attribution 4.0 International license. Further distribution of this work must maintain attribution to the author(s) and the published article's title, journal citation, and DOI.

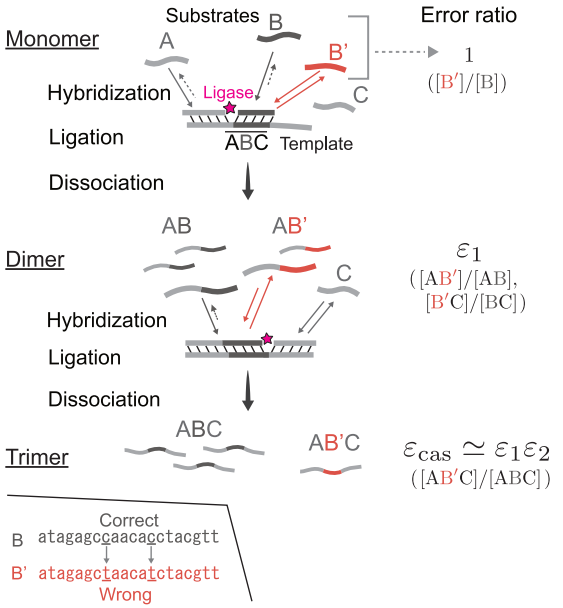


FIG. 1. Cascade replication by templated ligation. A, B, B′, and C are 20-nt DNA oligomers. Two strands adjacently hybridize (bind) to a template strand and are covalently connected by a ligase enzyme. Inset: Wrong substrate B′ has two nucleotide mutations indicated by underlines, which reduce the hybridization stability and also the ligation rate.

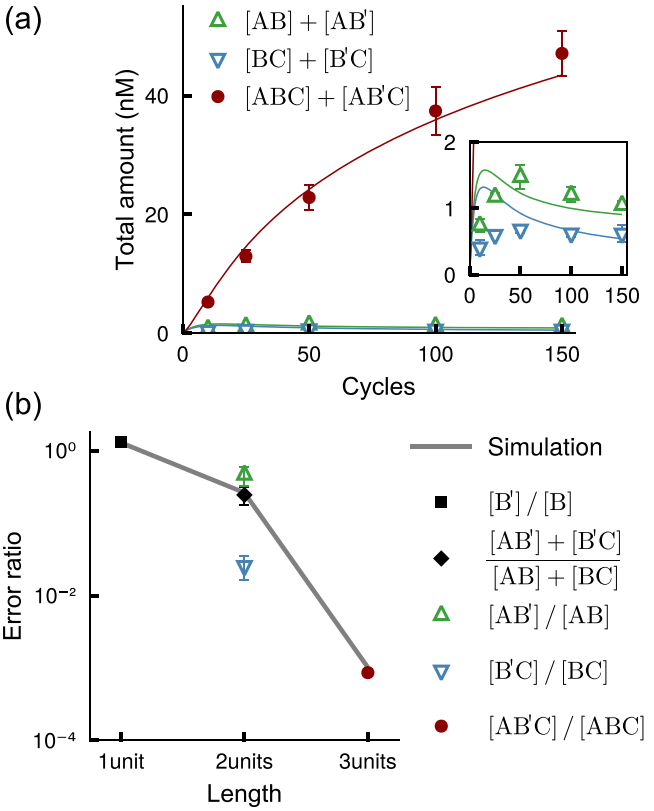


FIG. 2. Replication dynamics at $T_{\text{anneal}} = 66.0\,^{\circ}\text{C}$. (a) Dynamics of product concentrations: ABC + AB′C (red), AB + AB′ (green), and BC + B′C (blue). Solid curves are simulations with six fitting parameters, the hybridization rate k_{on}, the free energy change for the wrong monomer $\Delta G^{\circ}_{\text{mono,W}}$, and four types of ligation rates k_{L} corresponding to the connections AB, BC, AB′, and B′C (see Sec. V G). The inset is a magnified view of low concentrations. $N = 3$ or 4 independent experiments are averaged. (b) Single-site error ratios after 150 cycles (symbols) and the simulation (solid curves). The error bars correspond to the standard errors.

on a template (Fig. 1; see Sec. V for details). We mixed substrate DNA strands, template DNA strands, and thermostable DNA ligase in a total reaction volume of 20 µl (Sec. V A) and repeated a two-step thermal cycle using a thermal cycler (Sec. V B). The cycle consists of a denaturing step at 90 °C for 5 s and an annealing step at temperatures T_{anneal} ranging from 64.8 to 70.5 °C for 20 s. The thermal cycling is intended to increase product amounts by suppressing product inhibition. The substrate strands consist of 20-nt "monomer" sequences A, A′, B, B′, and C. Wrong substrates A′ and B′ contain two-nucleotide mutations relative to A and B, respectively. The 60-nt "trimer" template sequence, $\overline{\text{ABC}}$, is complementary to ABC. Here, $\overline{\cdot}$ denotes the complementary sequence and is described from the 3′ to 5′ ends. The substrate combinations vary from experiment to experiment. The initial concentrations of each substrate and template are 200 nM and 5 nM, respectively. The wrong substrate is mixed so that its fraction becomes 50% while maintaining the total concentration at 200 nM. We measured the length-dependent product amounts by denaturing polyacrylamide gel electrophoresis (denaturing PAGE; Sec. V C). Then, we extracted DNA from the gel and quantified the error ratio, defined as the ratio of wrong to correct product amounts, using quantitative PCR (qPCR; Sec. V D).

A. Replication dynamics

We measured the replication dynamics with a substrate combination $\mathcal{M}_{\text{cas}} = \{\text{A}, \text{B}, \text{B}', \text{C}\}$ (Fig. 2). This is the simplest system to realize the cascade replication of the template sequence information. The substrates are ligated on the template and form dimeric intermediate products AB (AB′) and BC (B′C). These dimers may dissociate from the templates and then rebind to other template strands. Finally, the dimers serve as the substrates and are ligated to form the final trimeric products ABC (AB′C). We observed that dimers accumulate at early cycles and gradually decrease thereafter [Fig. 2(a)]. This nonmonotonic dynamics of the intermediate products is a characteristic of cascade replication (Fig. 1) [15]. As reactions proceed, monomer concentrations decrease, which results in a decrease in the dimer production rate. Then, the dimer consumption by trimer formation outpaces the dimer production.

B. Error suppression

We found a significant decrease in the error ratio with increasing product length [Fig. 2(b)]. This is in sharp contrast to a *naive* chain-growth polymerization, in which the error ratio at each site is independent of sequence length.

We modeled the experimental system using ordinary differential equations based on mass-action kinetics (Sec. V F), incorporating hybridization, dissociation, ligation reactions, and thermal cycling with experimentally determined

parameters. The free energy change ΔG° associated with the correct hybridization of the sequences involving B was measured by the melting curve analysis. The ligation rates (k_L), the hybridization rate (k_{on}), and ΔG° for wrong hybridization involving B′ were obtained by fitting the model to experimental data [Fig. 2(a)]. The length-dependent dissociation rates (k_{off}) were determined so that they satisfy the detailed balance condition, $k_{on}/k_{off} = e^{-\Delta G^\circ/k_B T}$, where k_B is the Boltzmann constant.

The simulation successfully reproduced the experimental results, including the nonmonotonic growth of dimeric strands and decrease in error with the strand length (Fig. 2, solid curves). The difference in ΔG° between monomers B and B′ is approximately $\Delta\Delta G = -1.4\,k_B T$, corresponding to an equilibrium error ratio of $\exp(\Delta\Delta G/k_B T) = 0.24$, at 66.0 °C (Sec. V G). The observed error ratio for the final trimer product, [AB′C]/[ABC] = 0.00086, is far smaller than this value, indicating a nonequilibrium discrimination mechanism. We use a square bracket $[\cdot]$ for the molar concentration throughout the paper. Error ratio of monomer is larger than one because of the greater consumption of B over B′. The difference in the error ratios of AB and BC mostly originates from the difference in the ligation rates. Mutations in the strand with its 3′-end ligated greatly reduce the ligation efficiency compared to the mutations in the other strand [20].

C. Error suppression at individual steps

To investigate how the error propagates through cascade steps, we measured error incorporation at individual steps using substrate combinations $\mathcal{M}_1 = \{A, B, B'\}$ and $\mathcal{M}_2 = \{A, BC, B'C\}$, corresponding to the first and second steps of the cascade, respectively, in addition to $\mathcal{M}_{cas}$ [Fig. 3(a)]. We denote the corresponding single-site error ratios of the final products ([AB′]/[AB] for $\mathcal{M}_1$ and [AB′C]/[ABC] for $\mathcal{M}_2$ and $\mathcal{M}_{cas}$) as ε_1, ε_2, and ε_{cas}, respectively. We found that the error ratio with cascade reaction, ε_{cas}, is significantly lower than those of its elementary steps, ε_1 and ε_2. Importantly, $\varepsilon_{cas} \ll \varepsilon_2$ despite the fact that the cascade replication with $\mathcal{M}_{cas}$ and the one-step replication with $\mathcal{M}_2$ produce the same final products ABC and AB′C. This implies that cascade replication implements an error suppression mechanism. With cascade replication, dimer products dissociate after ligation in the first step. The amounts of these dimers are strongly biased toward AB and BC over AB′ and B′C, since $\varepsilon_1 \ll 1$. Because these dimers serve as substrates in the second step, the bias propagates to the next step, further reducing the error ratio in a multiplicative manner.

We compared the product $\varepsilon_1\varepsilon_2$ to the observed cascade error ratio, ε_{cas} (see Fig. S5(a) of the Supplemental Material [26]). Although there is a slight deviation in absolute values, the similarity between the two quantities suggests that ε_{cas} can be reasonably approximated by $\varepsilon_1\varepsilon_2$. This trend indicates that the concentration bias established in the first replication stage is effectively propagated to the second stage.

We found that ε_1 has a minimum around 66.6 °C and ε_2 has a minimum at T_{anneal} larger than 70.5 °C. This dependence occurs because the difference in hybridization stability between correct and wrong sequences is most pronounced at T_{anneal} close to their melting temperatures: $T_m = 64.5$ °C for B and 75.6 °C for BC (Sec. V E). These trends are quantitatively reproduced by simulations [curves in Fig. 3(a)]. Here, we assumed that the ligation rate k_L and hybridization rate k_{on} are constant, independent of T_{anneal} for simplicity. The deviation between simulations and experiments is significant at high T_{anneal}, possibly due to the above approximation of the temperature dependence of k_L and k_{on}, and implies the applicability limit of the simulation model.

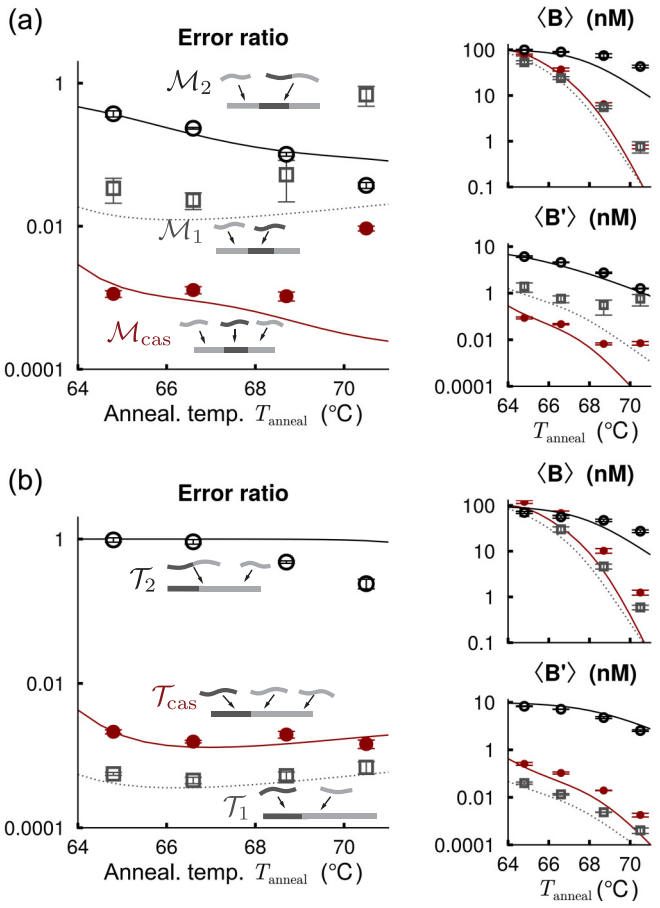


FIG. 3. Single-site error ratios (left) and product concentrations (right) after 150 cycles for the middle (a) and terminal (b) errors. ⟨B⟩ and ⟨B′⟩ denote the amount of the products containing B and B′ units, respectively (e.g., ⟨B⟩ = [AB] for $\mathcal{M}_1$ and ⟨B⟩ = [ABC] for $\mathcal{M}_2$ and $\mathcal{M}_{cas}$). Error bars indicate standard errors. Curves in panel (a) are simulation results. The parameters are obtained by fitting the dynamics [see Fig. 2(a)]. For panel (b), k_L for the A′B connection was additionally estimated. We assumed that k_L and k_{on} do not depend on T_{anneal}.

D. Kinetic proofreading

We derive the factor that determines the efficacy of error discrimination. The errors occur when the wrong substrates are fixed by ligation before dissociating from the templates. The dissociation occurs spontaneously in the reaction step with rates k_{off} or is forced in the denaturing step after the reaction step, with a duration of $\tau = 20$ s. Assuming that binding takes place immediately after the reaction step starts, the average duration until the dissociation becomes $(1 - e^{-k_{off}\tau})/k_{off}$. We define an effective dissociation rate as its

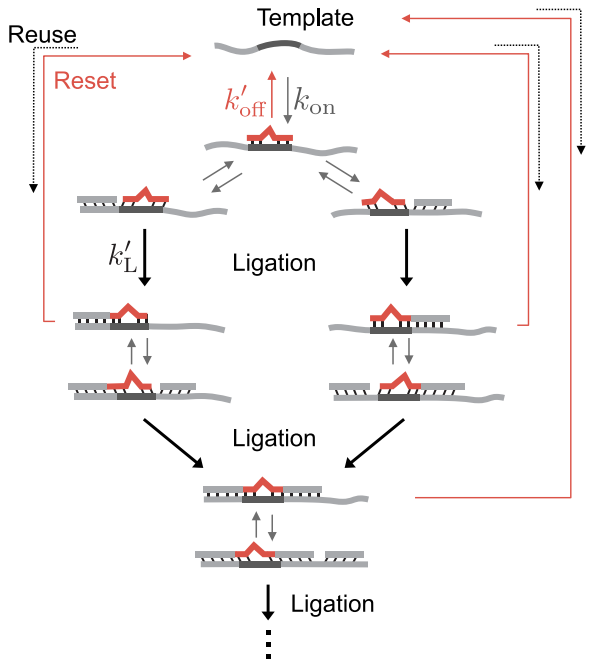


FIG. 4. Kinetic proofreading in ligation. The diagram is drawn with a focus on a specific template strand, and only the main reaction pathway involving a wrong substrate is shown. The loop structures that reset the state are characteristic of the kinetic proofreading [24]. The "Reuse" process indicates the hybridization of intermediate products.

inverse $\widetilde{k}_{\rm off} \equiv k_{\rm off}/(1-e^{-k_{\rm off}\tau})$. Hence, error discrimination is expected when a criterion, $k_{\rm L}/\widetilde{k}_{\rm off} > k'_{\rm L}/\widetilde{k}'_{\rm off}$, is satisfied. Here, $k'_{\rm L}$, $k'_{\rm off}$, and $\widetilde{k}'_{\rm off}$ are the rates for the reactions involving wrong substrates. We define an error discrimination factor f and rewrite this criterion as

$$f \equiv \frac{k_{\rm L}}{k'_{\rm L}}\frac{\widetilde{k}'_{\rm off}}{\widetilde{k}_{\rm off}} > 1. \tag{1}$$

The fitting of simulation curves to the experiments gives $k_{\rm L}/k'_{\rm L} \simeq 11.7$ for the ligation between A and B (B′) and 113 for that between B (B′) and C, independent of the substrate length (Sec. V G). The experiments also give $\widetilde{k}'_{\rm off}/\widetilde{k}_{\rm off} \sim 7$ for monomers and ∼1 for dimers (Sec. V H). Since most dimers do not dissociate during the reaction step because of their stable hybridizations, $\widetilde{k}'_{\rm off}$ and $\widetilde{k}_{\rm off}$ of dimers are similar to $1/\tau$, giving a ratio close to 1. Thus, we expect significant error discrimination with $\mathcal{M}_1$ and $\mathcal{M}_2$ since both exhibit $f \gg 1$. These arguments indicate that error is kinetically discriminated through the slower ligation and faster dissociation of wrong substrates. The error ratio after each cascade step is determined by the product of f and the concentration ratio of the correct to the wrong substrates. As this happens at each cascade step, the concentration becomes increasingly biased toward the correct one in a multiplicative way through the cascades.

This multiplicative error suppression mechanism with kinetic error discrimination is called the kinetic proofreading mechanism (Fig. 4) [22–24]. In our system, the virtually irreversible process of ligation provides the free-energy dissipation necessary for the discrimination. From each intermediate state, the state is reset by the dissociation of intermediate prodcuts. The dissociated intermediates may hybridize to the template again. This reusing, which is not implemented in the original Hopfield-Ninio kinetic proofreading [22,23], may increase the replication speed [24].

E. Terminal error

We evaluated also the terminal error by introducing A′ instead of B′; $\mathcal{T}_{\rm cas} = \{{\rm A}, {\rm A}', {\rm B}, {\rm C}\}$, $\mathcal{T}_1 = \{{\rm A}, {\rm A}', {\rm B}\}$, and $\mathcal{T}_2 = \{{\rm AB}, {\rm A}'{\rm B}, {\rm C}\}$ [Fig. 3(b)]. The cascade replication with $\mathcal{T}_{\rm cas}$ shows significantly smaller errors than the one-step replication with $\mathcal{T}_2$, implying the effectiveness of the cascade replication in reducing terminal errors.

We found a correlation between the product $\varepsilon_1\varepsilon_2$ and $\varepsilon_{\rm cas}$ (see Fig. S6 of the Supplemental Material [26]), supporting the cascade replication. Interestingly, $\varepsilon_2 \backsimeq 1$, particularly at low $T_{\rm anneal}$, and consequently, $\varepsilon_{\rm cas} \backsimeq 1$. This is because $\widetilde{k}'_{\rm off}/\widetilde{k}_{\rm off} \sim 1$, due to the stable hybridization of dimers (Sec. V H), and $k'_{\rm L}/k_{\rm L} \sim 1$, as the mutation is located far from the ligation site and thus does not significantly inhibit the reaction. Note that there are two reaction pathways for $\mathcal{T}_{\rm cas}$: ${\rm A}' + {\rm B} + {\rm C} \to {\rm A}'{\rm B} + {\rm C} \to {\rm A}'{\rm BC}$ and ${\rm A}' + {\rm B} + {\rm C} \to {\rm A}' + {\rm BC} \to {\rm A}'{\rm BC}$. In the latter, error discrimination does not occur at the first ligation step, potentially compromising the overall stringency of error suppression in cascade replication as $\varepsilon_{\rm cas} > \varepsilon_1$. Indeed, the simulation shows that about 60% of reactions follow this less discriminative pathway under the present conditions.

III. RESULTS—NUMERICAL SIMULATIONS

We investigate general situations with template strands of length $l \geqslant 4$, which may involve a cascade of more than two steps, by simulation (Sec. V I). We built the simulation model by extending the rate equations used for the fitting in Fig. 2, but with a different parameter set to evaluate the essential feature of the error suppression mechanism in long sequences. For simplicity, thermal cycling was not introduced. For comparison, we also modeled a chain-growth polymerization, where the hybridization and dissociation of only monomers are considered. This was implemented by a constraint that, once an intermediate is formed, it remains bound to the template without dissociation.

A. Single-site error

First, for simplicity, we simulate a simple case where an error occurs only at the central site of the sequence [i.e., the $(l/2)$th site for even l] [Fig. 5(a)]. Two hypothetical parameter sets were used: one with high monomer hybridization stability ($\Delta G^{\circ}_{\rm mono,R} = -10\,k_{\rm B}T$) and another with low stability ($-5\,k_{\rm B}T$), while keeping the energy difference between correct and wrong monomers fixed at $\Delta\Delta G = 1k_{\rm B}T$, which defines the ratio $k'_{\rm off}/k_{\rm off} = \exp(\Delta\Delta G/k_{\rm B}T) = 2.7$. In experiments, the monomer hybridization stability can be controlled by changing, for example, the monomer length, sequence, and temperature. Here, thermal cycling was not implemented for simplicity; hence, we used the total reaction time as τ to calculate the effective dissociation rates $\widetilde{k}_{\rm off}$ and $\widetilde{k}'_{\rm off}$.

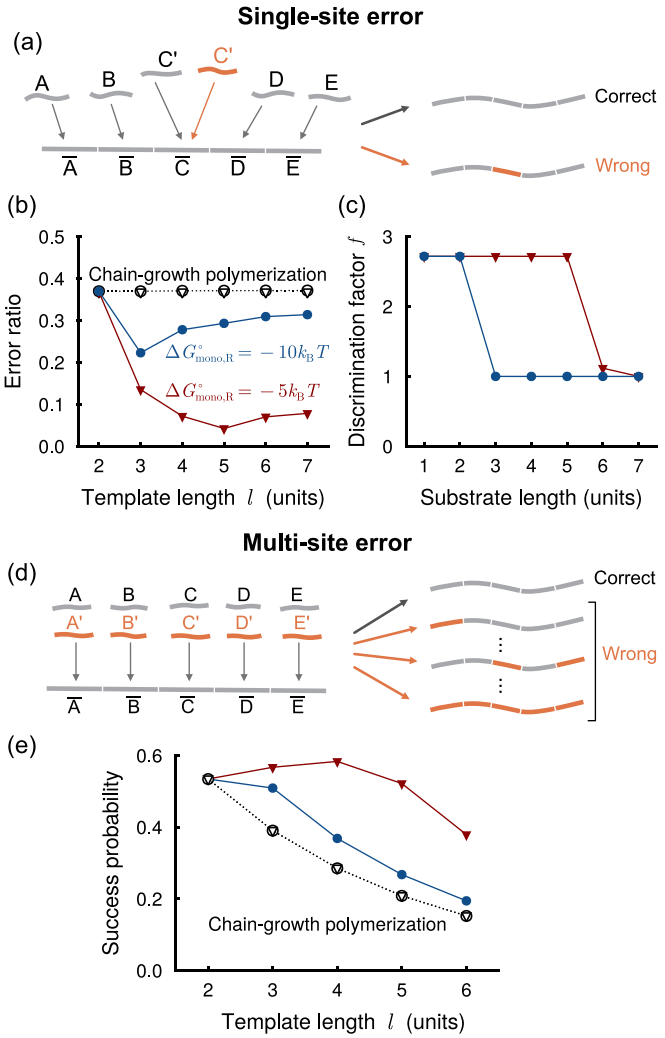


FIG. 5. Simulations of long-template replications with single-site errors [panels (a)–(c)] and multisite errors [panels (d) and (e)]. Cascade replication with stable monomer hybridization (blue closed circle) and less stable one (red closed triangle) with $\Delta\Delta G = 1\,k_\mathrm{B}T$, and corresponding conditions of chain-growth polymerization (open circle and triangle), are compared in panels (b), (c), and (e) (Sec. V I). (a) Schematic of single-site error replication, where an error may occur at the central position in a template of length l. The example of $l = 5$ is illustrated. (b) Error ratio. The error ratio for chain-growth polymerization is given by the product of $\exp(-\Delta\Delta G/k_\mathrm{B}T)$ and $k'_\mathrm{L}/k_\mathrm{L}$ and is 0.37, where $\Delta\Delta G = 1\,k_\mathrm{B}T$ and $k'_\mathrm{L}/k_\mathrm{L} = 1$ are assumed. (c) Discrimination factor f defined by Eq. (1) for each length of substrates. (d) Schematic of multisite error replication. Errors can occur at any site. (e) Success probability of replication in the multisite error case.

Across all tested conditions, cascade replication consistently exhibits lower error ratios than chain-growth polymerization for $l \geqslant 3$ [Fig. 5(b)]. In chain-growth polymerization, the error ratio is given by the discrimination factor f in Eq. (1) with the parameters for monomers, since dissociation of intermediates is not considered, and the fraction of the wrong monomers is set to be 50%. In cascade replication by ligation, the error ratio steeply decreases between $l = 2$ and 3 and then slowly increases with high monomer stability or further decreases with low stability. Thus, error suppression by cascade replication remains effective for longer sequences, particularly under conditions where hybridization is less stable.

The dependence of the error ratio on l is explained by the discrimination factor f [Fig. 5(c)]. Short strands have large k_off and hence $\tilde{k}_\mathrm{off} \simeq k_\mathrm{off}$, leading to $f \simeq k'_\mathrm{off}/k_\mathrm{off} = 2.7$. Long strands have small k_off and, therefore, $\tilde{k}_\mathrm{off} \simeq \tau$, leading to $f \simeq 1$. The threshold length dividing the two regimes depends on $\Delta G^\circ_{\mathrm{mono,R}}$. As replication progresses, intermediate products become longer and more stable, and hence the discrimination becomes less effective. Another important factor to consider is that longer templates are replicated via multiple pathways (e.g., A + BCD, AB + CD, or ABC + D for replicating ABCD). The efficacy of the discrimination depends on the pathway, and the number of possible pathways rapidly increases with the length. Therefore, characterising error suppression in the replication of long strands is not straightforward.

B. Multisite errors

We further examined a more generalized case in which mutations can occur at any position of the product sequence [Fig. 5(d)], using the same hybridization stability conditions tested in Fig. 5(b). In this scenario, replication of a template of length l generates up to 2^l distinct product species (Sec. V I). We define the success probability as the fraction of the correct (mutation-free) product among all 2^l final products [Fig. 5(e)]. We found that the cascade replication achieves higher success probabilities than chain-growth polymerization for $l \geqslant 3$. In both, the success probability decreases with l, consistent with the trends observed for the single-site error [Fig. 5(b)].

IV. DISCUSSION

Templated ligation is attracting interest as a plausible primitive replication mechanism, capable of generating rich replication dynamics despite its simplicity [10,14–19]. Previous studies have suggested that ligation is effective in preserving sequence information through higher-order replication in situations where both sides of the double strands are replicated [15,16,19]. In our experiments, we focused on the elementary replication steps, where only one strand of the double-stranded DNA is replicated. We demonstrated that templated ligation inherits a kinetic proofreading mechanism that suppresses errors through a cascade of kinetic error discrimination steps (Fig. 4) and leads to reduced errors with length in certain length ranges [Fig. 5(e)]. This has prominent implications for the study of the origin of life, where replication of a long sequence with fidelity is necessary for developing complex functions. Importantly, this mechanism does not require any external intervention, such as dilution or thermal cycling, as shown in Fig. 5. In the present experiments, we introduced thermal cycling to prevent the product inhibition, in which ligated products occupy the template and prevent it from templating further ligations. Thermal cycling is effective in increasing the product amounts but reduces the error discrimination effect by introducing τ, which reduces f

given by Eq. (1), implying a trade-off between amount and fidelity.

To characterize the essence of error discrimination, we used relatively long-sequence monomers with symmetric mutations in the middle of the sequence, which minimizes the influence of the ligase-specific bias. Mutations near either monomer-strand end will slow down the ligation at this end due to reduced efficiency in forming the phosphodiester bond [27] or due to an end flap [12]. The effect of such asymmetric ligation speed as well as nonenzymatic ligations [21] on the kinetic proofreading mechanism remains unclear and is a topic for future study.

From a bioengineering perspective, the kinetic proofreading by the cascade ligation has potential practical applications, including the genotyping by the so-called ligation detection reaction [13] and the production of long strands with fidelity for DNA storage technologies [28]. In addition, the concept of hierarchical assembly, which resembles cascade replication, appears in the field of macromolecular self-assembly [29]. Our findings may offer a perspective on these systems by providing a methodology to build more accurate assemblies.

V. METHODS

A. DNA sequences

DNA oligonucleotides with either a reverse-phase cartridge or PAGE purification grade were purchased from IDT or Eurofins Genomics (see Table S1 of the Supplemental Material for the sequences [26]). Substrates B, B′, C-X, BC-X, and B′C-Y were phosphorylated. The template $\overline{\mathrm{ABC}}$ (written from 3′ to 5′ ends) consists of 74 bases, consisting of three 20-base domains for substrate hybridization and 7-base overhangs at both ends. These seven-base overhangs are essential for distinguishing the template DNA from the products in PAGE analysis. The substrates were U-A, B, B′, and C-X for $\mathcal{M}_{\mathrm{cas}}$, U-A, B, and B′ for $\mathcal{M}_1$, and U-A, BC-X, B′C-Y, for $\mathcal{M}_2$. For the terminal error case, we used U-A, U′−A′, B, and C-X for $\mathcal{T}_{\mathrm{cas}}$, U-A, U′−A′, and B for $\mathcal{T}_1$, and U-AB, U′−A′B, and C-X for $\mathcal{T}_2$. The sequence A′ and B′ contains a two-base mutation relative to substrates A and B, respectively. Tag sequences U, U′, X, and Y correspond to primer-binding regions used in the quantitative PCR (qPCR) experiments (Sec. V D).

B. Ligation experiment

The reaction mixture had a total volume of 20 μl, containing 640 units m^{-1} L of thermostable Taq DNA ligase (New England Biolabs, MA, USA), 1× Taq DNA ligase buffer, 5 nM of the template $\overline{\mathrm{ABC}}$, and each substrates at the total substrate concentration of 200 nM. When A and A′ or B and B′ are mixed, each substrate was added at a concentration of 100 nM so that [A] + [A′] = 200 nM or [B] + [B′] = 200 nM. The thermal cycling was done with an initial 5 s denaturation step at 90 °C, followed by 20 s incubation steps at five different temperatures: 64.8, 66.0, 66.6, 68.7, and 70.5 °C under a real-time PCR cycler (CFX96, Bio-Rad). After the thermal cycling, an equal volume of loading buffer, consisting of 10 M urea and 240 mM ethylenediaminetetraacetic acid (EDTA) dissolved in 1× Tris-borate-EDTA buffer (TBE buffer, T3913, Sigma-Aldrich), was added to ensure the complete stop of the reaction.

C. Measurement of product amount

Following the thermal cycling, we quantified the amount of product using denaturing PAGE with a constant voltage of 200 V in a chamber immersed in a water bath at 70 °C. The gel contains 12.9% 19:1 acrylamide/bis-acrylamide 7 M urea, 120 mM EDTA, and 1× TBE. The gel was stained with 1× SYBR Gold (Thermo Fisher Scientific) dissolved in 1× TBE buffer. Gel images were captured using a 16-bit fluorescence scanner (LI-COR) (Fig. S1(a) of the Supplemental Material [26]).

The gel images were processed and analyzed using a laboratory-developed Python code using the OpenCV library [30]. Each lane was cropped into a rectangular region, and the fluorescence intensity of each pixel was averaged along the direction orthogonal to the lane. This yielded a one-dimensional intensity profile for each lane (Fig. S1(b) of the Supplemental Material [26]). To remove background noise, we applied the rolling minimum method [31] and subtracted the resulting background signal from the raw intensity data. The remaining signal peaks, corresponding to DNA products, were fitted using a Gaussian mixture model. The intensity of each peak was quantified as the area under the corresponding Gaussian curve. A calibration curve relating fluorescence intensity to DNA mass was generated in each gel by using reference bands (Fig. S1 of the Supplemental Material [26]).

After imaging the gel, DNA was extracted from each product band. The gel around a target band was excised and transferred into microtubes (DNA LoBind, Eppendorf), crushed, mixed with ultrapure water, and incubated at 37 °C for 1 h in a thermostatic shaking incubator. The supernatant was collected for qPCR measurement (Sec. V D).

D. Measurement of error ratio

We quantified the error ratio by performing qPCR measurements on the supernatant obtained from the DNA extraction step using a real-time PCR cycler (CFX96, Bio-Rad). We assumed that the concentration ratio between the correct and wrong products in the supernatant remained unchanged from the original sample prior to PAGE. The qPCR reaction mixture contains the supernatant sample, 200 nM of each primer (Table S2 of the Supplemental Material [26]), and Luna Universal qPCR Master Mix (New England Biolabs). The thermal cycling protocol consists of an initial denaturation step at 95 °C for 15 s, followed by an annealing step at either 65 °C or 50 °C for 30 s, and an extension step at 72 °C for 10 s. The fluorescence data were analyzed to determine the threshold cycle (Ct values) by the method described in Ref. [32].

For each experimental condition, we established independent calibration curves by measuring the Ct values of reference template strands with various concentrations prepared by serial dilutions with a ratio of 1/8 (Fig. S2 and Table S3 of the Supplemental Material [26]). The Ct values were fitted by $\mathrm{Ct} = -a \log_8(c/c_0) + b$, where c is the template concentration and $c_0 = 1$ pM is the reference concentration. a

and b are the fitting parameters (Table S4 of the Supplemental Material [26]).

E. Melting curve experiment

The melting curve experiment was conducted to determine the thermodynamic parameters of DNA hybridization for the simulations. We mixed DNA strands (100 nM for each strand), 0.25× SYBR Green I fluorescent dye for monitoring the concentrations of double-stranded DNA, and 1× Taq DNA ligase reaction buffer (New England Biolabs), consistent with the conditions used in the main experiments. To prevent nonspecific hybridizations, the tag sequences were not used for the monomer strands (see Table S5 of the Supplemental Material [26]). We gradually decreased the temperature of the sample in a stepwise manner from 90 °C to 30 °C by 0.2 °C every 15 s and measured the fluorescence in each step (see Fig. S3 of the Supplemental Material [26]).

The resulting fluorescence data were processed by using the exponential background removal method [33]. The normalized melting curves $\alpha(T)$ were obtained by linearly scaling the background-corrected fluorescence data between 0 and 1 using the maximum and minimum fluorescence values. Normalization was carried out within a manually selected temperature range that encompassed the melting transition of each curve. The standard free energy change, $\Delta G^\circ(T)$, was estimated from the normalized fluorescence signal $\alpha(T)$. Assuming that $\alpha(T)$ (see Fig. S3(b) of the Supplemental Material [26]) corresponds to the fraction of double-stranded DNA, $\Delta G^\circ(T)$ was calculated as $\Delta G^\circ(T) = k_B T \ln[2c(1-\alpha(T))^2/\alpha(T)]$, where $c = 100$ nM is the concentration of each DNA strand. $\Delta G^\circ(T)$ was then fitted by a function $\Delta H^\circ - T\Delta S^\circ$ to determine the standard enthalpy ΔH° and the standard entropy ΔS°, which are assumed to be independent of T. This leads to the dissociation constant $K_d = k_{off}/k_{on} = \exp(\Delta H^\circ/k_B T - \Delta S^\circ/k_B)$. The results are summarized in Table S6 of the Supplemental Material [26].

We observed a linear dependence of ΔH° and ΔS° on the strand length i for both correct and wrong substrates (see Fig. S4 of the Supplemental Material [26]); $\Delta H^\circ_{R/W}(i) = \phi_H\, i + \psi_{H,R/W}$ and $\Delta S^\circ_{R/W}(i) = \phi_S\, i + \psi_{S,R/W}$. Subscripts R and W refer to correct and wrong monomers. The slopes (ϕ_H and ϕ_S) were chosen in common between the correct and wrong monomers, representing the stabilization effect per sequence unit. The differences in intercepts ($\psi_{H,W} - \psi_{H,R}$ and $\psi_{S,W} - \psi_{S,R}$) represent the thermodynamic destabilization effect caused by hybridization error. The results are summarized in Table S6 of the Supplemental Material [26].

F. Numerical simulations

We constructed a model based on ordinary differential equations to simulate the experimental results, which incorporated hybridization, dissociation, ligation, and thermal cycling.

We modeled hybridization as a second-order reaction with an association rate constant k_{on}, which was assumed to be independent of DNA length [34] and temperature [35]. Up to three monomers can bind to the template strand.

The dissociation rate constant is denoted as $k_{off,i,j}$, where i represents the hybridization length in the unit of substrate monomers ($1 \leqslant i \leqslant l$), and j ($0 \leqslant j \leqslant i$) denotes the number of errors in the substrate sequence. l is the template length. The dissociation rate is given by

$$k_{off,i,j} = k_{on} K_{d,i,j} = k_{on} \exp(\Delta G^\circ_{i,j}/k_B T_{anneal}), \tag{2}$$

where $\Delta G^\circ_{i,j}$ is given by

$$\Delta G^\circ_{i,j} = \Delta G^\circ_{mono,R} + (i-1)(\phi_H + T_{anneal}\phi_S) + j\Delta\Delta G. \tag{3}$$

$\Delta\Delta G = \Delta G^\circ_{mono,W} - \Delta G^\circ_{mono,R}$ originates from the destabilization by a single error. We denote $\Delta G^\circ_{1,0}$ and $\Delta G^\circ_{1,1}$ as $\Delta G^\circ_{mono,R}$ and $\Delta G^\circ_{mono,W}$, respectively. The values of $\Delta G^\circ_{mono,R/W} = \Delta H^\circ_{R/W}(i=1) - T_{anneal}\Delta S^\circ_{R/W}(i=1)$, ϕ_H, and ϕ_S were obtained from the melting curve experiments.

The rate constants of the ligation k_L were chosen depending on the sequences of the terminals to be ligated. For example, $k_{L,AB}$ is used for the ligation of A and BC, and $k_{L,BC}$ is used for the ligation of A′B and C. For simplicity, we assumed that k_L is independent of temperature.

An example of the rate equation is

$$\begin{aligned}\frac{d[A, B : \overline{ABC}]}{dt} &= k_{on}[A : \overline{ABC}][B] + k_{on}[A][B : \overline{ABC}] \\ &\quad + k_{off,1,0}[A, B, C : \overline{ABC}] - k_{on}[A, B : \overline{ABC}][C] \\ &\quad - 2k_{off,1,0}[A, B : \overline{ABC}] - k_{L,AB}[A, B : \overline{ABC}].\end{aligned} \tag{4}$$

Here, colon (:) indicates the hybridized complex; e.g., A, B : $\overline{ABC}$ is the complex such that A and B are hybridized on a template $\overline{ABC}$.

We simulated the thermal cycling by repeating the calculation of the dynamics for a duration of $\tau = 20$ s at T_{anneal} and the disssociation of all the double-stranded DNAs, which corresponds to the denaturing.

G. Fitting of the dynamics data in experiments by simulation curves

To test the validity of our simulation, we fitted the simulation curves to the experimental curves of the dynamics measurement [Fig. 2(a)]. The fitting parameters are k_{on}, $\Delta G^\circ_{mono,W}$, $k_{L,AB}$, $k'_{L,AB'}$, $k_{L,BC}$, and $k'_{L,B'C}$, which will be collectively denoted as p. We obtained $\Delta G^\circ_{mono,W}$ as a fitting parameter, since the evaluation of $\Delta G^\circ_{mono,W}$ from the melting curve is not simple, unlike $\Delta G^\circ_{mono,R}$, due to the significant difference between $T_{anneal} = 66.0$ °C and the melting temperature of B′ : $\overline{B}$ ($T_M = 51.8$ °C). The temperature dependence of ΔH° is negligible only when T_{anneal} and T_M are similar when evaluating ΔG°.

We numerically integrated the rate equations and fitted the simulation curves to the experimental results by minimizing a cost function defined by

$$C(\{\mu\}, \{\sigma\}|p) = \sum_m \left[\left(\frac{\mu_{m,a} - f_{m,a}(p)}{\sigma_{m,a}} \right)^2 \left(\frac{\mu_{m,e} - f_{m,e}(p)}{\sigma_{m,e}} \right)^2 \right]. \tag{5}$$

Here, $\mu_{m,\mathrm{a/e}}$ and $\sigma_{m,\mathrm{a/e}}$ are the averages and standard errors of the total concentration (a) and the error ratio of the product with length m in experiments (b), respectively. $f_{m,\mathrm{a/e}}$ are the values of the numerical simulations. The minimization was done using the Nelder-Mead method [36] implemented by the Optimization.jl package of Julia [37].

We obtained $k_{\mathrm{on}} = 9.41 \times 10^6\ \mathrm{M^{-1}s^{-1}}$, $\Delta G^{\circ}_{\mathrm{mono,W}} = -8.15\ \mathrm{kcal^{-1}\,mol^{-1}}$, $k_{\mathrm{L,AB}} = 0.222\ \mathrm{s^{-1}}$, $k'_{\mathrm{L,AB'}} = 0.0190\ \mathrm{s^{-1}}$, $k_{\mathrm{L,BC}} = 0.207\ \mathrm{s^{-1}}$, and $k'_{\mathrm{L,BC'}} = 0.001\,84\ \mathrm{s^{-1}}$. We discuss the validity of the obtained parameters below. The value of k_{on} was in the order of 10^6, which aligns with the experimentally obtained values reported in some previous literature [11,35,38,39]. It is difficult to validate the ligation rates based on reference values because the actual concentration of active ligase is not accessible in experiments, and the ligation rate of the Taq DNA ligase with internal mismatches has not been reported for the present experimental condition. On the other hand, the specificity ratios, defined by the ratio of the correct and wrong ligation rates, were $k_{\mathrm{L,AB}}/k'_{\mathrm{L,AB'}} = 11.7$ and $k_{\mathrm{L,BC}}/k'_{\mathrm{L,B'C}} = 113$. These values are compatible with the previous report that the specificity ratios are $\geqslant 8$ for an internal mismatch at various mismatch positions [27]. The fact that the value for $\mathrm{B'} + \mathrm{C}$ is approximately ten times larger than that for $\mathrm{A} + \mathrm{B'}$ could be attributed to the nature of ligase that the mismatch at the 3′ side has a larger discrimination ability than the mismatch at the 5′ side, as was previously reported [20].

H. Simulations of individual-step experiments

We simulated the experiments in Fig. 3 by using the same model as in the dynamics experiment (Sec. V G). For the middle errors [Fig. 3(a)], we used the parameters described in Sec. V G. For the terminal errors [Fig. 3(b)], we need additional parameter $k'_{\mathrm{L,A'B}}$, which was estimated to be $k'_{\mathrm{L,A'B}} = 5.51 \times 10^{-4}$ by manual fitting of the experimental results in Fig. 3(b) by simulations. This value is significantly smaller than $k'_{\mathrm{L,AB'}}$ and $k'_{\mathrm{L,B'C}}$. This difference could be caused by the geometry of the error site. As noted above, the specificity ratio increases when the error is positioned at the 3′ side of the ligation site [20].

I. Simulations with long templates

The template concentration was fixed at 1 nM and the total substrate concentration at each binding domain was set to 40 nM. To maintain this total, we mixed 20 nM of the correct monomer with 20 nM of the wrong monomer. The hybridization rate k_{on} was set to $10^7\ \mathrm{M^{-1}s^{-1}}$. For simplicity, k_{L} was fixed at $10\ \mathrm{s^{-1}}$ across all cases, regardless of whether an error was present, its position, or the length of the substrate. We stopped the simulations when the total concentration of final products, including both correct and wrong sequences, reached a specific threshold value, which was determined depending on $\Delta G^{\circ}_{\mathrm{mono,R}}$; 0.0001 pM for $\Delta G^{\circ}_{\mathrm{mono,R}} = -5\,k_{\mathrm{B}}T$ and 1 pM for $-10\,k_{\mathrm{B}}T$. The length-dependent error ratio was calculated as $\varepsilon(l) = w_l/r_l$, where r_l and w_l are the concentrations of the correct and wrong final products, respectively, with the length of l.

For the chain-growth polymerization, we set $k_{\mathrm{off},i,j} = 0$ for $i \geqslant 2$, allowing only monomer hybridization and dissociation while preventing intermediate dissociation.

For the simulations in Fig. 5(e), we used the same setup as in the single-site error simulations. The only difference is that the errors are allowed at any site.

ACKNOWLEDGMENTS

We thank Yohei Nakayama for the helpful discussion. This work was supported by JSPS KAKENHI Grant No. JP23K17658 and JST ERATO Grant No. JPMJER2302 (all to S.T.), and JST SPRING Grant No. JPMJSP2114, Japan (to H.A.).

DATA AVAILABILITY

The data that support the findings of this article are not publicly available upon publication because it is not technically feasible and/or the cost of preparing, depositing, and hosting the data would be prohibitive within the terms of this research project. The data are available from the authors upon reasonable request.

[1] P. Schuster and M. Eigen, *The Hypercycle: A Principle of Natural Self-Organization* (Springer, Berlin, 1979).

[2] E. Domingo, R. A. Flavell, and C. Weissmann, *In vitro* site-directed mutagenesis: Generation and properties of an infectious extracistronic mutant of bacteriophage Qβ, Gene **1**, 3 (1976).

[3] E. Domingo, D. Sabo, T. Taniguchi, and C. Weissmann, Nucleotide sequence heterogeneity of an RNA phage population, Cell **13**, 735 (1978).

[4] D. R. Mills, R. L. Peterson, and S. Spiegelman, An extracellular Darwinian experiment with a self-duplicating nucleic acid molecule, Proc. Natl. Acad. Sci. USA **58**, 217 (1967).

[5] D. M. Whiley and T. P. Sloots, Sequence variation in primer targets affects the accuracy of viral quantitative PCR, J. Clin. Virol. **34**, 104 (2005).

[6] A. A. Gibriel and O. Adel, Advances in ligase chain reaction and ligation-based amplifications for genotyping assays: Detection and applications, Mutat. Res. Rev. Mutat. Res. **773**, 66 (2017).

[7] D. Andrieux and P. Gaspard, Nonequilibrium generation of information in copolymerization processes, Proc. Natl. Acad. Sci. USA **105**, 9516 (2008).

[8] P. Sartori and S. Pigolotti, Thermodynamics of error correction, Phys. Rev. X **5**, 041039 (2015).

[9] T. E. Ouldridge and P. Rein ten Wolde, Fundamental costs in the production and destruction of persistent polymer copies, Phys. Rev. Lett. **118**, 158103 (2017).

[10] J. Y. Matsubara, T. Nobuto, and K. Kaneko, Avoidance of error catastrophe via proofreading innate to template-directed polymerization, Phys. Rev. Res. **5**, 013170 (2023).

[11] H. Aoyanagi, S. Pigolotti, S. Ono, and S. Toyabe, Error-suppression mechanism of PCR by blocker strands, Biophys. J. **122**, 1334 (2023).

[12] T. Takahashi, H. Aoyanagi, S. Pigolotti, and S. Toyabe, Blocking uncertain mispriming errors of PCR, Biophys. J. **123**, 3558 (2024).

[13] F. Barany, Genetic disease detection and DNA amplification using cloned thermostable ligase, Proc. Natl. Acad. Sci. USA **88**, 189 (1991).

[14] P. W. Anderson, Suggested model for prebiotic evolution: The use of chaos, Proc. Nat. Acad. Sci. USA **80**, 3386 (1983).

[15] S. Toyabe and D. Braun, Cooperative ligation breaks sequence symmetry and stabilizes early molecular replication, Phys. Rev. X **9**, 011056 (2019).

[16] P. W. Kudella, A. V. Tkachenko, A. Salditt, S. Maslov, and D. Braun, Structured sequences emerge from random pool when replicated by templated ligation, Proc. Natl. Acad. Sci. USA **118**, e2018830118 (2021).

[17] J. H. Rosenberger, T. Göppel, P. W. Kudella, D. Braun, U. Gerland, and B. Altaner, Self-assembly of informational polymers by templated ligation, Phys. Rev. X **11**, 031055 (2021).

[18] G. Laurent, T. Göppel, D. Lacoste, and U. Gerland, Emergence of homochirality via template-directed ligation in an RNA reactor, PRX Life **2**, 013015 (2024).

[19] A. V. Tkachenko and S. Maslov, Spontaneous emergence of autocatalytic information-coding polymers, J. Chem. Phys. **143**, 045102 (2015).

[20] J. Luo, D. E. Bergstrom, and F. Barany, Improving the fidelity of Thermus thermophilus DNA ligase, Nucleic Acids Res. **24**, 3071 (1996).

[21] L. Zhou, D. K. O'Flaherty, and J. W. Szostak, Template-directed copying of RNA by non-enzymatic ligation, Angew. Chem., Int. Ed. **59**, 15682 (2020).

[22] J. J. Hopfield, Kinetic proofreading: A new mechanism for reducing errors in biosynthetic processes requiring high specificity, Proc. Natl. Acad. Sci. USA **71**, 4135 (1974).

[23] J. Ninio, Kinetic amplification of enzyme discrimination, Biochimie **57**, 587 (1975).

[24] A. Murugan, D. A. Huse, and S. Leibler, Speed, dissipation, and error in kinetic proofreading, Proc. Natl. Acad. Sci. USA **109**, 12034 (2012).

[25] R. Mukherjee, A. Sengar, J. Cabello-García, and T. E. Ouldridge, Kinetic proofreading can enhance specificity in a nonenzymatic DNA strand displacement network, J. Am. Chem. Soc. **146**, 18916 (2024).

[26] See Supplemental Material at http://link.aps.org/supplemental/10.1103/pdhn-ncpl for supplementary methods and results.

[27] C. E. Pritchard and E. M. Southern, Effects of base mismatches on joining of short oligodeoxynucleotides by DNA ligases, Nucleic Acids Res. **25**, 3403 (1997).

[28] A. Doricchi, C. M. Platnich, A. Gimpel, F. Horn, M. Earle, G. Lanzavecchia, A. L. Cortajarena, L. M. Liz-Marzán, N. Liu, R. Heckel, R. N. Grass, R. Krahne, U. F. Keyser, and D. Garoli, Emerging approaches to DNA data storage: Challenges and prospects, ACS Nano **16**, 17552 (2022).

[29] W.-S. Wei, A. Trubiano, C. Sigl, S. Paquay, H. Dietz, M. F. Hagan, and S. Fraden, Hierarchical assembly is more robust than egalitarian assembly in synthetic capsids, Proc. Natl. Acad. Sci. USA **121**, e2312775121 (2024).

[30] G. Bradski, The OpenCV library, Dr. Dobb's J. Software Tools **120**, 122 (2000).

[31] P. Yaroshchyk and J. E. Eberhardt, Automatic correction of continuum background in laser-induced breakdown spectroscopy using a model-free algorithm, Spectrochim. Acta B **99**, 138 (2014).

[32] G. J. Boggy and P. J. Woolf, A mechanistic model of PCR for accurate quantification of quantitative PCR data, PLoS One **5**, e12355 (2010).

[33] R. Palais and C. T. Wittwer, Mathematical algorithms for high-resolution DNA melting analysis, in *Methods in Enzymology*, Computer Methods, Part A (Academic Press, Cambridge, 2009), Vol. 454, pp. 323–343.

[34] K. Tawa, D. Yao, and W. Knoll, Matching base-pair number dependence of the kinetics of DNA–DNA hybridization studied by surface plasmon fluorescence spectroscopy, Biosens. Bioelectron. **21**, 322 (2005).

[35] J. X. Zhang, J. Z. Fang, W. Duan, L. R. Wu, A. W. Zhang, N. Dalchau, B. Yordanov, R. Petersen, A. Phillips, and D. Y. Zhang, Predicting DNA hybridization kinetics from sequence, Nat. Chem. **10**, 91 (2018).

[36] J. A. Nelder and R. Mead, A simplex method for function minimization, Comput. J. **7**, 308–313 (1965).

[37] V. K. Dixit and C. Rackauckas, Optimization.Jl: A unified optimization package, Zenodo (2023), https://zenodo.org/records/7738525.

[38] M. Weitz, J. Kim, K. Kapsner, E. Winfree, E. Franco, and F. C. Simmel, Diversity in the dynamical behavior of a compartmentalized programmable biochemical oscillator, Nat. Chem. **6**, 295 (2014).

[39] B. Yurke and A. P. Mills, Using DNA to power nanostructures, Genet. Program. Evolvable Mach. **4**, 111 (2003).